Rita Crasta, H. Naik*, S. V. Suryanarayana, Ganesh Sanjeev, P. M. Prajapati, M. Kumar, T. N. Nathaniel, V. T. Nimje, K. C. Mittal, and A. Goswami

Photo-neutron cross-section of ^{96}Zr using bremsstrahlung radiation with end point energies of 10 and 12.5 MeV

Abstract: The ^{96}Zr$(\gamma, n)^{95}$Zr reaction cross-section was experimentally determined at end point bremsstrahlung energies of 10 and 12.5 MeV using off-line γ-ray spectrometric technique. The cross-section increases sharply from the end point energy of 10 to 12.5 MeV, which indicates the role of excitation energy. The reaction cross-section as a function of photon energy was also calculated theoretically using the TALYS 1.2 computer code. The flux weighted average value of the ^{96}Zr$(\gamma, n)^{95}$Zr reaction cross-section for the end-point bremsstrahlung energies of 10 and 12.5 MeV was also calculated using the experimental and theoretical data of mono-energetic photons to compare with the present data. The cross-section given in the present work at end- point bremsstrahlung energy of 10 MeV is closer to the flux-weighted value of TALYS but higher than the literature data. On the other hand, at 12.5 MeV, it is higher than the flux weighted value of TALYS and the literature data.

Keywords: ^{96}Zr$(\gamma, n)^{95}$Zr reaction cross-sections, ^{197}Au$(\gamma, n)^{196}$Au flux monitor, End point bremsstrahlung energy of 10 and 12.5 MeV, Off-line γ-ray spectrometric technique, TALYS calculation .

————

*Corresponding Author: H. Naik, Radiochemistry Division, Bhabha Atomic Research Centre, Mumbai 400 085, India, E-Mail: naikhbarc@yahoo.com

Rita Crasta, Ganesh Sanjeev: Microtron Centre, Department of Studies in Physics, Mangalore University, Mangalagangotri 574199, Karnataka, India

T. N. Nathaniel, A. Goswami: Radiochemistry Division, Bhabha Atomic Research Centre, Mumbai 400 085, India

S. V. Suryanarayana: Nuclear Physics Division, Bhabha Atomic Research Centre, Mumbai-400085, India

P. M. Prajapati: Physics Department, Faculty of Science, The M S University of Baroda, Vadodara 390 002, India

M. Kumar, V. T. Nimje, K. C. Mittal: Accelerator & Pulse Power Division, Bhabha Atomic Research Centre, Mumbai 400 085, India

1 Introduction

The cross-section data of the nuclear reactions induced by different photon energies are required for applied nuclear physics, nuclear models, elemental analysis and reactor technology [1]. Reliable cross-section data for the production of residual nuclides by medium-energy photon-, proton- and neutron-induced reactions are essential for accelerator driven sub-critical system (ADSs) to calculate the radioactive inventories of the spallation target, cladding material and structural materials [2–5]. Among the structural materials, zirconium and its alloys are important cladding materials for various types of reactors [6] due to its low neutron absorption cross-section [7–10]. Zirconium is a very strong malleable, ductile, lustrous, grayish-white metal having high resistance to corrosion in aggressive environments such as alkalis, acids, salt water and the other agents even at high temperatures. Thus Zr metal has many applications, such as heat exchangers, pumps, reactor vessels, valves, surgical appliances and chemical industry, where corrosive agents are employed [11]. In reactor application, alloy of Zr containing Sn, Fe and Cr with or without Ni is used as Zircaloy-2 and Zircaloy-4. These four elements have very low neutron absorption cross-sections. So they do not affect the neutron economy of the reactor, but allow the zirconium alloy to meet the required engineering criteria for cladding and assembly components. Zircaloy-2 contains 1.5% tin, 0.1% iron, 0.1% chromium, 0.05% nickel, and not more than 0.01% nitrogen, whereas Zircaloy-4 differs from Zircaloy-2 by lower nickel content (0.007%). Zircaloy-2 is used in boiling water reactors (BWR) and zircaloy-4 in pressurized water reactors (PWR) [12]. In pressurized heavy water reactors (PHWR), Zr-2.5 wt % Nb alloy is used as pressure tubes [13–15]. Zircaloy can be also used as cladding material in ADSs [2, 16]. However, in ADSs along with high-energy neutrons, high-energy photons are also produced during spallation process, which can cause different types of nuclear reactions of the cladding and structural materials. Thus it is important to measure the neutron- and

photon-induced reaction cross-sections of structural (Fe, Ni, Cr et.) and cladding (Zr) materials.

Accurate photo-nuclear cross-sections near the reaction thresholds are insufficient because of experimental difficulties [17]. Nonetheless high quality evaluated photonuclear cross-sections have been compiled for many elements [1]. A number of workers [18–21] reported data on photon-induced reaction cross sections for zirconium isotopes using the activation technique but they are only for mono-energetic photons. Only one set of data is available on ^{96}Zr(γ, n) reaction using mono-energetic photon beam [22]. However, there is no data on the ^{96}Zr$(\gamma, n)^{95}$Zr reaction cross-section at bremsstrahlung of any energy. In a reactor and particularly in ADSs, the photons produced are bremsstrahlung radiations over wide range of energies. Thus the bremsstrahlung induced reaction cross-section of Zr is of primary interest for reactor design. In view of this, in the present work, we determine the ^{96}Zr$(\gamma, n)^{95}$Zr reaction cross-section at end-point bremsstrahlung energies of 10 and 12.5 MeV using activation followed by off-line γ-ray spectrometric technique. The ^{96}Zr$(\gamma, n)^{95}$Zr reaction cross-section induced by 10 and 12.5 MeV bremsstrahlung was also calculated theoretically using the computer code TALYS 1.2 [23] and compared with experimental data of the present work.

2 Experimental details

The experiment was carried out using electron linear accelerator of the Electron Beam Centre (EBC) at Kharghar, Navi Mumbai, India. In the present work, the electron LINAC was operated at 10 and 12.5 MeV. Two sets of irradiation were done for end point bremsstrahlung energies of 10 and 12.5 MeV to measure the cross-section of ^{96}Zr$(\gamma, n)^{95}$Zr reaction. In both the set of experiments, ^{nat}Zr and ^{nat}Au metal target foils were used for irradiation. The bremsstrahlung was generated when a pulsed electron beam hits a 0.25 mm thick tantalum (Ta) target. The Ta target was placed on a suitable stand at 3.0 cm distance from the electron beam exit window and the samples were kept at a distance of 10 cm from the tantalum target. A schematic diagram of the sample stack (Zr-Au) for irradiation along with the electron to bremsstrahlung converter is shown in Figure 1.

The isotopic abundance of ^{96}Zr in the ^{nat}Zr sample is 2.8%, whereas ^{197}Au is mono-isotopic. High purity ^{nat}Zr and ^{197}Au metal target foils were wrapped with 0.025 mm thick super pure aluminum foil. In the first set of experiment the weights of the zirconium and gold foils were 0.2379 and 0.0525 g, respectively. In the second set of
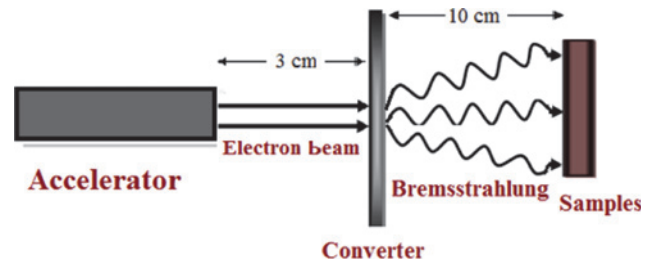

Fig. 1: Schematic diagram showing the arrangement used for the production of bremsstrahlung irradiation.

experiment, the weights of Zr and Au were 0.1808 and 0.1297 g, respectively. The high purity gold metal foil was used to measure the bremsstrahlung flux.

Different sets of targets for ^{96}Zr and ^{197}Au were made for different irradiations. Each of the target samples was placed below the tantalum foil for individual irradiation. The target assembly was irradiated separately for 4–5 h with end-point bremsstrahlung energies of 10 and 12.5 MeV. In the 10 MeV bremsstrahlung irradiation, the electron LINAC was operated with a pulse repetition rate (PRR) of 310 Hz, a pulse width of 10 μs and the average beam current of 33 mA. On the other hand, in the 12.5 MeV bremsstrahlung irradiation the electron LINAC was operated with a PRR of 300 Hz, a pulse width of 10 μs and the average beam current of 25 mA. After the irradiation, the samples were cooled for 2–3 h. Then, the irradiated targets of Zr and Au foil along with the Al wrapper were mounted on different Perspex plates and taken for γ-ray counting.

The γ-ray counting of the reaction products from ^{96}Zr and ^{197}Au was done by using an energy-and efficiency-calibrated 80 cm^3 HPGe detector coupled to a PC based 4K-channel analyzer. The resolution of the detector system was 2.0 keV at 1332.0 keV of ^{60}Co. The energy-and efficiency-calibration of the detector system was done by counting the γ-ray energies of a standard ^{152}Eu source. The dead time of the detector system was kept below 10% by placing the irradiated sample at a suitable distance from the detector to avoid the pile up effects.

3 Data analysis

The net photo peak areas (A_{net}) of the γ-rays of nuclides of interest were calculated after subtracting the linear Compton background from their total peak areas. The radionuclide ^{95}Zr was identified through characteristic γ-lines of 724.2 and 756.7 keV. Thus the ^{96}Zr$(\gamma, n)^{95}$Zr reaction cross-section ($\langle\sigma\rangle$) at the end-point bremsstrahlung ener-

Table 1: Nuclear spectroscopic data of the radionuclides ^{196}Au and ^{95}Zr produced by the (γ, n) reactions on ^{nat}Au and ^{nat}Zr [24–27] along with the reaction Q-value and threshold energy.

Nuclide	Half-life	γ-ray energy (keV)	γ-ray abundance (%)	Reaction	Q-value (MeV)	Threshold energy (MeV)
^{196}Au	6.183 d	332.98	22.9	^{197}Au(γ, n)	−8.0723	8.0725
		355.69	87			
		426.0	7			
^{95}Zr	64.02 d	724.2	44.17	^{96}Zr(γ, n)	−7.8563	7.8566
		756.73	54			
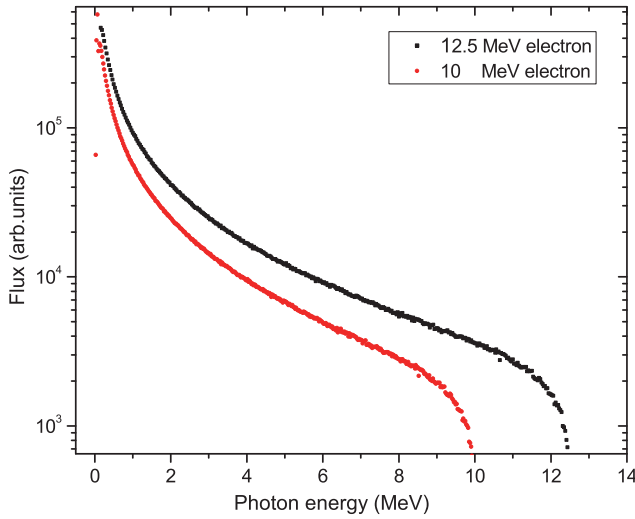
Fig. 2: Plot of bremsstrahlung spectrum with end-pint energies of 10 and 12.5 MeV [28].

Fig. 3: Plot of experimental [32] and theoretical [23] ^{197}Au$(\gamma, n)^{196}$Au reaction cross-section as a function of photon energy.

gies of 10 and 12.5 MeV were obtained from the net peak areas of the full energy photo-peaks using the following equation.

$$A_{(net)} \left(\frac{CL}{LT} \right) = \frac{N \langle\sigma\rangle \Phi a \varepsilon (1 - e^{-\lambda t})(e^{-\lambda T})(1 - e^{-\lambda CL})}{\lambda} \tag{1}$$

where N is the number of target atoms, Φ is the photon flux, "a" is the branching intensity of the analyzed γ-ray and ε is detection efficiency for the γ-line of interest. "t" and T are the irradiation and cooling times, whereas CL and LT are the clock time and live time of counting, respectively.

In Eq. (1) the CL/LT term has been used for dead time correction. The γ-ray energies and the decay data for the residual nuclide such as branching ratio, half-lives are taken from Refs. [24, 25] and are given in Table 1. The photon flux (Φ) was determined from the net photo-peak activity (A_{net}) of the 355.7 keV γ-line of ^{196}Au from ^{197}Au(γ, n) reaction [26, 27] and using the rearranged Eq. (1). The average cross-section ($\langle\sigma\rangle$) for ^{197}Au(γ, n) reaction was cal-
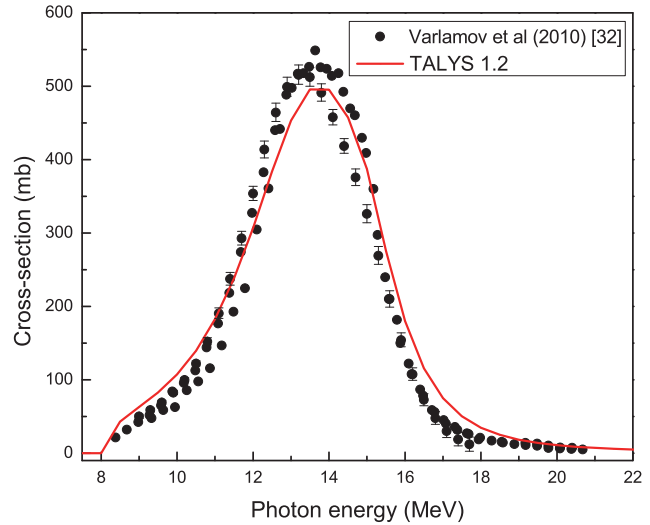
culated using the following relation

$$\langle\sigma\rangle = \frac{\sum \sigma \Phi}{\sum \Phi} \tag{2}$$

For end point bremsstrahlung energy of 10 and 12.5 MeV, the photon flux distribution was calculated by using the EGS4 code [28]. The photon flux (Φ) distribution with respect to photon energy (E) is presented in Figure 2. Sufficient ^{197}Au$(\gamma, n)^{196}$Au reaction cross-section (σ) data based on mono-energetic photons are available in literature [29–32]. In the present experiment we have taken the (γ, n) cross-section of ^{197}Au reaction from Ref. [32], which is shown in Figure 3. ^{197}Au$(\gamma, n)^{196}$Au reaction cross-section as a function of photon energy was also calculated theoretically using the computer code TALYS 1.2 [23] and the result is plotted in the same Figure 3 for comparison. The flux-weighted $\langle\sigma\rangle$ values for the ^{197}Au$(\gamma, n)^{196}$Au reaction was obtained from the literature [32] and TALYS 1.2 [23] data and is listed in Table 2.

The photon flux for ^{197}Au$(\gamma, n)^{196}$Au reaction was used in Eq. (1) to calculate the average cross-section of

the ^{96}Zr$(\gamma, n)^{95}$Zr reaction. However, the photon flux for the ^{96}Zr$(\gamma, n)^{95}$Zr reaction differs slightly from the photon flux based on the ^{197}Au$(\gamma, n)^{196}$Au reaction due to different threshold values. The threshold values for the ^{197}Au$(\gamma, n)^{196}$Au and ^{96}Zr$(\gamma, n)^{95}$Zr reactions are 8.073 and 7.851 MeV, which were taken from the Ref. [33] and are presented in Table 1. The detailed calculations of flux ratio based on threshold values are given in Ref. [34].

4 Results and discussion

The average cross-section of the ^{96}Zr$(\gamma, n)^{95}$Zr reaction determined in the present work from the photo-peak activities of 724.2 and 756.7 keV γ-lines of ^{95}Zr at the end point bremsstrahlung energies of 10 and 12.5 MeV are presented in Table 2. The ^{96}Zr$(\gamma, n)^{95}$Zr reaction cross-sections are based on the bremsstrahlung flux obtained from flux-weighted ^{197}Au$(\gamma, n)^{196}$Au reaction cross-section of mono-energetic photons from literature [32] and TALYS [23]. The uncertainties associated with the experimental reaction cross-sections data are based on the replicate measurements. The overall uncertainty is the quadratic sum of both statistical and systematic errors. The random error in the observed activity is primarily due to counting statistics, which is estimated to be 5%–10%. This can be determined by accumulating the data for an optimum time period that depends on the half-life of nuclide of interest. The systematic errors are due to uncertainties in photon flux estimation ($\sim$ 2%), the irradiation time ($\sim$ 0.5%), the detection efficiency calibration ($\sim$ 3%), the half-life of the reaction products and the γ-ray abundances ($\sim$ 2%) as reported in the literature [24–27]. Thus the total systematic error is about $\sim$ 3.7%. The overall uncertainty is found to range between 6.2 and 10.7%, coming from the combination of a statistical error of 5%–10% and a systematic error of 3.7%.

It can be seen from Table 2 that the experimentally determined average ^{96}Zr$(\gamma, n)^{95}$Zr reaction cross-
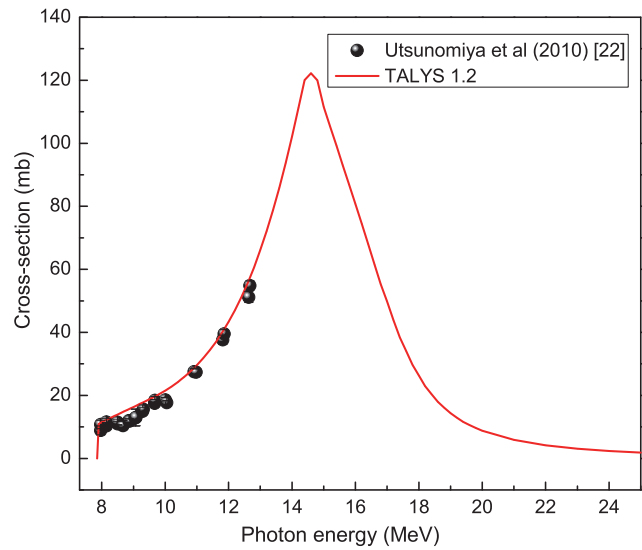

Fig. 4: Plot of experimental and theoretical ^{96}Zr$(\gamma, n)^{95}$Zr reaction cross-section as a function of photon energy.

section varies between 16.8 and 24.1 mb at the end-point bremsstrahlung energy of 10 and between 32.9 and 39.1 mb at 12.5 MeV. The variation in the cross-section is due to the use of two different type of photon flux based on experimental and theoretical ^{197}Au$(\gamma, n)^{196}$Au reaction cross-section. In literature, there is no experimental data on the ^{96}Zr$(\gamma, n)^{95}$Zr reaction cross-section at any end-point bremsstrahlung energy to compare with the present data. However, the cross-sections for the ^{96}Zr$(\gamma, n)^{95}$Zr reaction based on mono-energetic photons are available in Ref. [22], which are shown in Figure 4. The ^{96}Zr$(\gamma, n)^{95}$Zr reaction cross-section increases with mono-energetic photon energy up to 13 MeV. Since there is no measured data beyond 13 MeV, the ^{96}Zr$(\gamma, n)^{95}$Zr reaction cross-section as a function of photon energy above threshold value was calculated theoretically using the computer code TALYS code 1.2 [23], as explained in Ref. [34]. All possible outgoing channels for the given photon energy were considered. However, the cross-section for the (γ, n) reaction of

Table 2: Comparison of experimental ^{96}Zr$(\gamma, n)^{95}$Zr reaction cross-section with the flux-weighted average data based on mono-energetic photons from literature and TALYS at the end-point bremsstrahlung energies of 10 and 12.5 MeV.

Photon energy (MeV)	Flux-weighted ^{197}Au (γ, n) $\langle\sigma\rangle$ (mb) [Ref]	Flux (Φ) $\times 10^8$ (Photons/cm^2/s)	^{96}Zr$(\gamma, n)^{95}$Zr reaction cross-section ($\langle\sigma\rangle$ in mb)		
			Experimental	TALYS	Literature [Ref.]
10	38.65 [32]	13.65 ± 0.22	16.84 ± 0.98	15.29	12.33 [22]
	55 [23]	9.59 ± 0.16	24.16 ± 1.6		
12.5	95.35 [32]	4.16 ± 0.04	32.89 ± 1.59	21.7	17.49 [22]
	113.86 [23]	3.48 ± 0.03	39.07 ± 1.89		

^{96}Zr was specially looked for and collected. The calculated ^{96}Zr$(\gamma, n)^{95}$Zr reaction cross-section as a function of photon energy is also plotted in Figure 4. The theoretical curve agrees with the available experimental data [22] up to 13 MeV.

Using Eq. (2), the flux weighted average cross-section for ^{96}Zr$(\gamma, n)^{95}$Zr reaction was obtained from the mono-energetic data of literature [22] and TALYS [23] (see Table 2 for comparison). The experimentally determined ^{96}Zr$(\gamma, n)^{95}$Zr reaction cross-section at end-point bremsstrahlung energy of 10 MeV is closer to the flux-weighted value obtained from TALYS but is higher than the flux-weighted value from literature [22]. On the other hand, at the end-point bremsstrahlung energy of 12.5 MeV, the experimental value is higher than the flux weighted values of TALYS and literature [22]. The difference between the experimental and the flux-weighted TALYS and literature data may be due to the undefined bremsstrahlung spectrum from EGS4 code [28]. Further, it can be seen from Table 2 that the ^{96}Zr$(\gamma, n)^{95}$Zr reaction cross-section from present work increases from $16.8-24.1$ mb at the end-point bremsstrahlung energy of 10 MeV to $32.9-39.1$ mb at 12.5 MeV. Similarly, the flux-weighted values from literature [22] and TALYS [23] based on mono-energetic photons also increase from the end-point bremsstrahlung energy of 10 MeV to 12.5 MeV. This observation indicates the effect of excitation energy.

5 Conclusions

The ^{96}Zr$(\gamma, n)^{95}$Zr reaction cross-sections at end-point bremsstrahlung energies of 10 and 12.5 MeV have been measured for the first time. The cross-section increases from 10 to 12.5 MeV indicating the role of excitation energy. The reaction cross-section as a function of photon energy was also calculated theoretically using the computer code TALYS 1.2. The experimentally determined ^{96}Zr$(\gamma, n)^{95}$Zr reaction cross-section at the end-point bremsstrahlung energy of 10 MeV is closer to the flux-weighted value of TALYS but higher than the literature data. On the other hand, at 12.5 MeV it is higher than the flux-weighted value of TALYS and literature data, which may be due to the use of theoretical bremsstrahlung spectrum.

References

1. IAEA-TECDOC-1178: Handbook on Photonuclear Data for Applications, Cross-sections and Spectra. Available online at: http://www-nds.iaea.org (2000).

2. Bowman, C. D.: Annu Rev. Nucl. Part. Sci. **48**, 505 (1998).

3. Chadwick, M. B., Hughes, H. G., Little, R. C., Pitcher, E. J., Young, P. G.: Progress in Nuclear Energy **38**, 179 (2001).

4. IAEA-TECDOC-985: Accelerator Driven Systems: Energy Generation and Transmutation of Nuclear Waste: Status Report. Available online at: http://www-nds.iaea.org (1998).

5. Ganesan, S.: Pramana J. Phys. **68**, 257 (2007).

6. Attar, F. M. D., Mandal, R., Dhole, S,D., Saxena, A., Ashokkumar, Ganesan, S., Kailas, S., Bhoraskar, V. N.: Nucl. Phys. A **802**, 1 (2008).

7. Zee, R. H., Guinan, M. W., Huang, J. S.: Journal of Nuclear Materials **141**–**143**, 874 (1986).

8. Stojilovic, N., Bender, E. T., Ramsier, R. D.: Progress in Surface Science **78**, 101 (2005).

9. IAEA TECDOC-1410: Delayed Hydride Cracking in Zirconium Alloys in Pressure Tube Nuclear Reactors, Final report of a coordinated research project. Available online at: http://www-nds.iaea.org (1998–2002).

10. Pansare, G. R., Dighe, P. M., Bhoraskar, V. N.: Radiat Phys. Chem. **40**, 213 (1992).

11. DOE Fundamentals Handbook Material Science, Volume 2 of 2 DOE-HDBK-1017/2-93 January, U. S. Department of Energy FSC-6910, Washington, D. C. 20585 (1993).

12. Anderson, E. T., Wilson, S. A., Schemel, J. H.: United States Patent, 4,908,071 (1990).

13. Patnaik, P.: Handbook of Inorganic Chemicals, The McGraw–Hill Companies, Printed in the United States of America, 995 (2003).

14. Shreir, L. L., Jarman, R. A., Burstein, G. T.: Corrosion, Vol. 1, Third Edition, Oxford: Butterworth-Heinemann (1994).

15. Rudling, P., Strasser, A., Garzarolli, F.: IZNA7 Special Topic Report Welding of Zirconium Alloys, ANT International, Krongjutarvagen 2C, SE-73 0 50 Skultuna, Sweden (2007).

16. Adam, J., Balabekyan, A. R., Barashenkov, V. S., Brandt, R., Golovatiouk, V. M., Kalinnikov, V. G., Katovsky, K., Krivopustov, M. I., Kumar, V., Kumawat, H., Odoj, R., Pronskikh, V. S., Solnyshkin, A. A., Stegailov, V. I., Tsoupko-Sitnikov, V. M., Westmeier, W.: Eur. Phys. J. A **23**, 61 (2005).

17. IAEA-EXFOR, Experimental Nuclear Reaction Data, Available online at: http://www-nds.iaea.org/exfor.
18. Veyssiere, A., Beil, H., Bergere, R., Carols, P., Fagot, J., Lepretre, A., de Miniac, A.: Z. Phys. A-Atoms and Nuclei **306**, 139 (1982).
19. Utsunomiya, H., Goriely, S., Kondo, T., Kaihoti, T., Makinaga, A., Goko, S., Akimune, H., Yamagata, T., Toyokawa, H., Mstsumoto, T., Harano, H., Hohara, S., Lui, Y.-W., Hilaire, S., Peru, S., Koning, A. J.: Phys. Rev. Lett. **100**, 162502 (2008).
20. Berman, B. L., Pywell, R. E., Dietrich, S. S., Thompson, M. N., Mc Neill, K. G., Jury, J. W.: Phys. Rev. C **36**, 1286 (1987).
21. Berman, B. L., Caldwell, J. T., Harvey, R. R., Kelly, M. A., Bramblett, R. L., Fultz, S. C.: Phys. Rev. **162**, 1098 (1967).
22. Utsunomiya, H., Goriely, S., Akimune, H., Harada, H., Kitatani, F., Goko, S., Toyokawa, H., Yamada, K., Kondo, T., Itoh, O., Kamata, M., Yamagata, T., Lui, Y-W., Hilaire, S., Koning, A. J.: Phys. Rev. C **81**, 035801 (2010).
23. Koning, A. J., Hilaire, S., Duijvestijn, M. C.: Proceedings of the International Conference on Nuclear Data for Science and Technology-ND 2004, AIP Vol.769, Edited by Haight, R. C., Chadwick, M. B., Kawano, T., Talou, P. (Santa Fe, 2005), p. 1154 (2004).
24. Browne, E., Firestone, R. B.: Table of Radioactive Isotopes, edited by Shirley, V. S., John Wiley & Sons, New York (1986).
25. Xiaolong, H.: Nuclear Data Sheets **108**, 1093 (2007).
26. Yoshinaga, O., Toyoaki, K., Nobuyoshi, S.: Bulletin of the Chemical Society of Japan **42**, 387 (1969).
27. Yamadera, A., Yoshitomo, U., Nakamura, T.: Nuclear Instruments and Methods in Physics Research A **329**, 188 (1993).
28. Nelson, W. R., Hirayama, H., Rogers, D. W. O.: Stanford Linear Accelerator Center (SLAC) report-265, The EGS4 Code system. Available at: www.slac.stanford.edu/pubs/slacreports/slac-r-265.html (1985).
29. Veyssiere, Beil, H., Bergere, R., Carlos, P., Lepretre, A.: Nuclear Physics A **159**, 561 (1970).
30. Vogt, K., Mohr, P., Babilon, M., Bayer, W., Galaviz, D., Hartmann, T., Hutter, C., Rauscher, T., Sonnabend, K., Volz, S., Zilges, A.: Nuclear Physics A **707**, 241 (2002).
31. Hara, K. Y., Harada, H., Kitatani, F., Goko, S., Ya Hohara, S., Kaihori, T., Makinaga, A., Utsunomiya, H., Toyokawa, H., Yamada, K.: J. Nucl. Sci. Tech. **44**, 938 (2007).
32. Varlamov, V. V., Ishkhanov, B. S., Orlin, V. N., Troshchiev, S. Yu.: Izv. Rossiiskoi Akademii Nauk, Ser. Fiz. **74**, 884 (2010).
33. Medsker, L. R., Horen, D. J.: Nuclear Data Sheets **B8**, 29 (1972).
34. Crasta, R., Naik, H., Suryanarayana, S. V., Prajapati, P. M., Jagadisan, K. C., Thakare, S. V., Ganesh, S., Nimje, V. T., Mittal, K. C., Goswami, A.: J. Radioanal. Nucl. Chem. **290**, 367 (2011).